JACS
JOURNAL OF THE AMERICAN CHEMICAL SOCIETY
Article
pubs.acs.org/JACS

Capturing the Hemoglobin Allosteric Transition in a Single Crystal Form

Naoya Shibayama,*[,†] Kanako Sugiyama,[‡] Jeremy R. H. Tame,[‡] and Sam-Yong Park[‡]

[†]Division of Biophysics, Department of Physiology, Jichi Medical University, 3311-1 Yakushiji, Shimotsuke, Tochigi 329-0498, Japan
[‡]Drug Design Laboratory, Graduate School of Medical Life Science, Yokohama City University, 1-7-29 Suehiro, Tsurumi, Yokohama, 230-0045, Japan

ABSTRACT: Allostery in many oligomeric proteins has been postulated to occur via a ligand-binding-driven conformational transition from the tense (T) to relaxed (R) state, largely on the basis of the knowledge of the structure and function of hemoglobin, the most thoroughly studied of all allosteric proteins. However, a growing body of evidence suggests that hemoglobin possesses a variety of intermediates between the two end states. As such intermediate forms coexist with the end states in dynamic equilibrium and cannot be individually characterized by conventional techniques, very little is known about their properties and functions. Here we present complete structural and functional snapshots of nine equilibrium conformers of human hemoglobin in the half-liganded and fully liganded states by using a novel combination of X-ray diffraction analysis and microspectrophotometric O_2 equilibrium measurements on three isomorphous crystals, each capturing three distinct equilibrium conformers. Notably, the conformational set of this crystal form varies according to shifts in the allosteric equilibrium, reflecting the differences in hemoglobin ligation state and crystallization solution conditions. We find that nine snapshot structures cover the complete conformational space of hemoglobin, ranging from T to R2 (the second relaxed quaternary structure) through R, with various relaxed intermediate forms between R and R2. Moreover, we find a previously unidentified intermediate conformer, between T and R, with an intermediate O_2 affinity, sought by many research groups over a period of decades. These findings reveal a comprehensive picture of the equilibrium conformers and transition pathway for human hemoglobin.

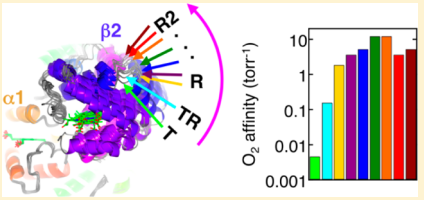

INTRODUCTION

Allostery allows protein molecules to regulate their functions rapidly and appropriately in response to external influences. Perhaps the most studied example is human hemoglobin, an $(\alpha\beta)_2$ tetrameric protein that binds O_2 cooperatively at the four heme sites. In the 1960s to 1980s, it was believed that the structural basis of hemoglobin allostery was firmly established by the identification of the two X-ray structures of the unliganded (deoxy) and liganded (oxy) form, that differ in the arrangement of two $\alpha\beta$ dimers by about 14° of dimer−dimer rotation,[1,2] most likely corresponding to the T and R states of the Monod−Wyman−Changeux (MWC) two-state allosteric model.[3] However, the current understanding of structure−function relationships in hemoglobin is less certain than it was 30 years ago. It has become apparent that hemoglobin shows multiple conformations in dynamic equilibrium, not only two.

The two-state model was challenged in the 1990s by two observations. One is the discovery of an alternate quaternary structure, R2, for liganded hemoglobin.[4] Modeling studies[5,6] have shown that in the T to R2 transition one dimer turns relative to the other by nearly 10° beyond R (Figure 1a), leading to suggestions that the R state is only a crystallographic artifact, but these have been strongly disputed.[7] More importantly, recent studies using X-ray crystallography,[8] NMR,[9] and solution X-ray scattering[10] have suggested very significant conformational flexibility of liganded hemoglobin in solution. However, structural and functional characterization of the individual conformers has been elusive because of the inherent difficulty of analyzing such unstable structures.

The second and more critical observation is the striking difference in the O_2 affinity of the T-state (K_T) between in solution and in crystals,[11] which cannot be reconciled with a simple two-state model. Whereas in solution K_T varies widely (approximately 50-fold) with solution conditions,[12] the O_2 affinity of the crystalline T-state is independent of solvent conditions and agrees with the lowest K_T value in solution (Figure 1b). The failure of the two-state model to account for experimental results from a wide variety of biophysical analyses has led several research groups to propose a putative intermediate affinity state between the canonical T and R states.[16−19] The structure that this intermediate might adopt, however, remains unresolved.

In this work, we show that the structures and functions of coexisting states can be determined in a single crystal form in which hemoglobin is free to adopt any allosteric structure, depending on the conditions, and at the same time allows O_2 binding to be monitored directly in the crystal. We identify a wide range of forms, providing a basis for understanding why two end crystal structures cannot adequately fit the experimental data from other solution-based techniques.[8−10] We also identify a new intermediate form with an intermediate O_2 affinity, which may

Received: January 13, 2014
Published: March 17, 2014

   dx.doi.org/10.1021/ja500380e | J. Am. Chem. Soc. 2014, 136, 5097−5105

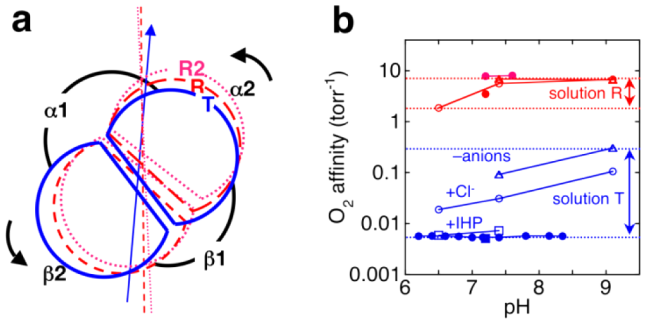

Figure 1. Structure and function of human hemoglobin. (a) Schematic diagram illustrating the movement of the $\alpha 2\beta 2$ dimer relative to the $\alpha 1\beta 1$ dimer on going from unliganded T (blue) to liganded R (red) or R2 (magenta). The $\alpha 1\beta 1$ dimers are superposed. The molecular dyad axes are also shown. (b) Comparison of changes in the O_2 affinities of hemoglobin in solution (open symbols)[12] and in crystals (filled symbols).[11,13−15] Colors are same as in (a). Open circles indicate the presence of 0.1 M Cl^-, and open triangles indicate a minimal anion concentration in the buffer solutions. For the T-state, squares indicate the presence of 2 mM inositol hexaphosphate (IHP) that stabilizes the lowest affinity state.[16] The data at 25 °C[12,13] or 15 °C[14] were converted to those at 20 °C using the reported enthalpy values.[12,13]

represent the putative intermediate allosteric state for human hemoglobin.[16−19]

EXPERIMENTAL SECTION

Sample Preparations. Human adult hemoglobin was prepared as previously described.[20] The cross-link agent bis(3,5-dibromosalicyl)-fumarate was synthesized and recrystallized twice from ethanol.[20] $\alpha 1\beta 2$ half-CO-liganded, cross-linked Fe(II)−Ni(II) hybrid hemoglobin (XL[α(Fe-CO)β(Ni)][α(Ni)β(Fe-CO)]) was prepared using appropriate parental hemoglobins as previously reported.[21] Met-hemoglobin was prepared according to the method of Benesch et al.[22] followed by passage through a column of Amberlite MB-3 (Rohm and Hass).

Crystallization. Crystallization was carried out at 20 °C using the microbatch method under paraffin oil. Crystals of XL[α(Fe-CO)β(Ni)][α(Ni)β(Fe-CO)] with phosphate (referred to as HL+) were obtained from CO-saturated 1.0% (w/v) XL[α(Fe-CO)β(Ni)][α(Ni)-β(Fe-CO)] solution containing 17% (w/v) PEG3350 in 10 mM potassium phosphate buffer pH 6.8. Similarly, crystals of XL[α(Fe-CO)β(Ni)][α(Ni)β(Fe-CO)] without phosphate (referred to as HL−) were obtained from CO-saturated 1.0% (w/v) XL[α(Fe-CO)β(Ni)]-[α(Ni)β(Fe-CO)] solution containing 19% (w/v) PEG3350 and 5% (v/v) glycerol with no buffer pH 7.6. Crystals of met-hemoglobin with phosphate (referred to as FL+) were obtained from 1.3% (w/v) met-hemoglobin solution containing 18% (w/v) PEG3350 and 5% (v/v) glycerol in 10 mM potassium phosphate buffer pH 6.8. For the HL+ and HL− crystals, the microbatch samples were sealed with CO gas inside a gas-barrier bag including Oxygen Absorbing System A-500HS (ISO, Yokohama, Japan) to ensure anaerobic conditions during crystallization. For all the crystals, the mother liquors containing 15% (v/v) glycerol were used as cryoprotectant in which the crystals were rinsed briefly before flash-freezing in liquid nitrogen.

Data Collection and Structure Determination. X-ray data were collected using the synchrotron radiation source at the beamline BL-17A station of the Photon Factory, Tsukuba, Japan. Diffraction data sets were integrated and scaled with HKL2000 and SCALEPACK.[23] Consistent with previous work,[24] the FL+ crystals belonged to the monoclinic space group C2, with unit cell constants of a = 227.6 Å, b = 56.1 Å, c = 141.6 Å, and β = 102.5°, and contained three tetramers in the asymmetric unit. Both of the HL− and HL+ crystals were also of the same C2 space group

Table 1. Crystal Parameters, Data Collection, and Structure Refinement

data Set	FL+	HL−	HL+
data collection statistics			
resolution range (Å)	50.0−2.75	50.0−2.80	50.0−2.50
space group	C2	C2	C2
unit cell dimensions (Å)	a = 227.62, b = 56.06, c = 141.56, β = 102.5°	a = 228.33, b = 55.53, c = 139.68, β = 103.1°	a = 228.94, b = 54.34, c = 137.88, β = 103.2°
reflections (measured/unique)	212,339/45,029	203,812/41,293	273,526/56,987
completeness (%)	98.2 (81.0)[a]	97.8 (83.0)[a]	98.9 (93.8)[a]
mean $\langle I\rangle/\langle\sigma(I)\rangle$	16.8	22.3	12.9
multiplicity	4.9	4.9	4.8
Rmerge (%)[b]	5.8 (43.1)[a]	5.8 (30.2)[a]	7.1 (43.3)[a]
B factor from Wilson plot (Å^2)	85	81	58
refinement statistics			
resolution range (Å)	20.0−2.75	20.0−2.80	20.0−2.50
R-factor (%)/free R-factor (%)[c]	25.1/28.7	25.9/28.7	26.7/29.2
Rms deviations from ideals			
bond lengths (Å)	0.009	0.009	0.009
bond angles (°)	1.451	1.472	1.478
B-values (all atoms)			
overall/mol-A/mol-B/mol-C	90/87/81/103	97/89/85/141	62/67/59/59
Ramachandran plot			
residues in most favorable regions (%)	82.0	83.5	85.5
residues in additional allowed regions (%)	17.3	16.1	13.9
residues in generously allowed regions (%)	0.7	0.4	0.6
PDB ID	4N7N	4N7O	4N7P

[a]Values in parentheses are for the highest resolution shell with a resolution of 2.80−2.75 Å (FL+), 2.85−2.80 Å (HL−), and 2.59−2.50 Å (HL+). [b]Rmerge = $\Sigma|I_i - \langle I\rangle|/\Sigma|I_i|$, where I_i is the intensity of an observation, $\langle I\rangle$ is the mean value for that reflection, and the summations are over all reflections. [c]R-factor = $\Sigma_h||F_o(h)| - |F_c(h)||/\Sigma_h F_o(h)$, where F_o and F_c are the observed and calculated structure factor amplitudes, respectively. The free R-factor was calculated with 5% of the data excluded from refinement.

dx.doi.org/10.1021/ja500380e | J. Am. Chem. Soc. 2014, 136, 5097−5105

Table 2. Quaternary States, O_2 Affinities, and Relative Spectral Contribution of Molecules A, B, and C in the HL+, HL−, and FL+ Crystals

molecule	dimer−dimer rotation[a] angle (deg)[b] / translation (Å)[c] / axis direction (deg)[d]	quaternary state	O_2 affinity ($Torr^{-1}$)	spectral contribution[e] (%)
HL+ A	19.11 (19.09)/3.4/22.2 (3.1)	near R2	3.8 ± 1.3	22.5
B	11.42 (11.41)/1.8/5.4 (19.4)	near R	3.8 ± 1.3	33.7
C	2.62 (2.82)/ −0.5/95.5 (119.3)	near T	0.0064 ± 0.0020	43.8 (37 ± 6)
HL− A	19.91 (19.90)/3.4/23.2 (2.1)	near R2	5.2 ± 0.6	21.5
B	11.09 (11.09)/2.2/13.6 (11.1)	between R and R2	5.2 ± 0.6	35.7
C	10.96 (10.84)/0.8/12.3 (29.0)	TR (between T and R)	0.16 ± 0.09	42.8 (47 ± 2)
FL+ A	17.14 (17.11)/3.2/19.2 (6.0)	between R and R2	12 ± 6	23.5
B	13.92 (13.92)/2.0/21.3 (3.5)	between R and R2	12 ± 6	30.3
C	12.45 (12.40)/2.1/7.4 (19.9)	near R	2 ± 8[f]	46.2 (48 ± 13)

[a]Dimer−dimer rotation from the T-state is determined for each tetramer, by first overlapping one dimer with one of the T-state (PDB ID 2DN2), and then fitting the other dimer pair. [b]Dimer−dimer screw rotation angle from the T-state. Values in parentheses are those for noncrystallographic symmetry equivalent dimer. The rotation angles for the R-state and R2-state are 14.1 and 22.9°, respectively. [c]Rotation translation from the T-state. The translation values for the R-state and R2-state are 1.3 and 3.3 Å, respectively. The negative value for molecule C in HL+ indicates the opposite direction to all other values in the table. [d]The angle between the rotation axis and that found for the R-state (or that found for the R2-state in parentheses). [e]Relative spectral contribution of the hemes in each molecule, calculated on the basis of the orientations of individual hemes in the crystal structures. In the cases of HL+ and HL−, randomly placed dimers are assumed. Values in parentheses are those calculated from the O_2 dissociation curves (shown in Figure 7a), according to the biphasic model (see Experimental Section). In crystals, the apparent O_2 saturation will depend on the heme orientation relative to the direction of the measuring light, because the heme planes do not project equally onto the optical axis of the measuring light. All of the spectra in this study were measured with light incident on the (010) crystal faces. [f]The estimate for molecule C of the FL+ crystal is not accurate because of the number of parameters (see Experimental Section).

with comparable cell parameters (see Table 1). All the structures were solved by molecular replacement using PHASER.[25] To minimize the model bias on the quaternary structure, the $\alpha\beta$ dimer (not the tetramer) of human oxyhemoglobin (PDB ID 2DN1)[26] was used as the initial search model. Using data between 20 and 3 Å, the orientations and positions of three tetramer hemoglobin molecules in an asymmetric unit were found and improved by rigid-body refinement. The models were refined with the simulated-annealing protocol using a bulk solvent correction with data between 20.0 and 2.75 Å resolution (FL+) or 20.0 and 2.8 Å resolution (HL−) or 20.0 and 2.5 Å resolution (HL+). Successive rounds of model rebuilding using COOT[27] were followed by refinement using CNS.[28] Validation of the final model was carried out using PROCHECK.[29] A summary of the data collection and refinement statistics is given in Table 1.

Difference Distance Matrices. Difference distance matrices of the $\alpha1\beta2$ subunits of each tetramer were calculated using the R-state CO-bound hemoglobin (PDB ID 2DN3)[26] as a reference by the program DDMP (Center for Structural Biology, Yale University, New Haven, CT, USA).

Overlap Method. The superpositions of different models were made using an in-house program based on the FIT procedure of Guoguang Lu.[25] RMSD values were calculated by fitting the Cα atoms of all residues except residue 1 of each chain (which is disordered in some models). 570 atoms were fitted in each tetramer fit. To find the dimer−dimer screw rotation angle, $\alpha\beta$ dimer pairs were fitted sequentially. The angle was derived twice by comparing different $\alpha\beta$ dimers from each tetramer, and the results were shown to be equal (to the quoted accuracy) in each case (Table 2).

O_2 Equilibrium Measurement. O_2 equilibrium curves of crystals were determined as described.[15] Among grown crystals, thin flat crystals having a well-developed (010) (or *ac*) crystal face were chosen for measurements. The crystals were washed with mother liquor containing 0.1 mg/mL of catalase (Sigma). For spectral measurements, a single crystal with about 20 μL of its mother liquor was placed on a cover glass and then sealed in a flow chamber mounted on the stage of a Ziess UMSP 80 microspectrophotometer. Since the met-hemoglobin (FL+) crystals do not bind O_2, they were reduced and converted to the ferrous CO-bound form, by washing with CO-saturated mother liquor containing 0.2% (w/v) sodium dithionite ($Na_2S_2O_4$), followed by CO-saturated mother liquor without sodium dithionite. Before measurements on all the crystals, removal of CO was carried out in the flow chamber with humidified O_2, at a gas flow of 10 mL/min, under illumination with white light. Humidified N_2−O_2 gas mixtures at defined partial O_2 pressures were prepared by a GB-4C gas blender (Kofloc, Japan) with modifications, and flowed into the chamber. The O_2 pressures were detected in the outflow from the chamber using a MC-7G-L galvanic O_2 sensor (Iijima, Japan). The absorption spectra of crystals equilibrated with different O_2 pressures at 21−22 °C were recorded between 450 and 700 nm with unpolarized light incident on (010) crystal face. According to the method of Mozzarelli et al.,[11] the fractional saturation of the ferrous hemes with O_2 (Y) was calculated by a least-squares fit of the observed absorption spectra to a linear combination of three reference spectra and a baseline offset. The reference spectra are the absorption spectra of crystals of oxy-, deoxy-, and met-forms of each hemoglobin sample. Since in the case of the FL+ crystals, increases in O_2 pressure above 380 Torr caused no appreciable spectral changes, the spectrum obtained under pure O_2 was taken as the reference spectrum for FL+. By contrast, because full O_2 saturation could not be attained for the HL− and HL+ crystals even under O_2 atmosphere, the data at the highest pressures were extrapolated to infinite O_2 pressure to obtain the oxy-form spectra by using double reciprocal plots of the O_2 pressure (p) and the absorbance change at p at each of the 251 wavelengths from 450 to 700 nm. After each O_2 equilibrium measurement, the crystal was reduced by washing with mother liquor containing 0.2% (w/v) sodium dithionite for the measurement of the deoxyhemoglobin reference spectrum. The crystal was then washed with mother liquor to remove sodium dithionite, followed by washing with mother liquor containing 5 mM potassium ferricyanide to oxidize the crystal for the measurement of the met-hemoglobin reference spectrum.

Determination of O_2 Affinity. According to the biphasic model (see Results and Discussion), O_2 dissociation curves were fitted using equation: $Y(p) = (1 - C)Y_{AB}(p) + CY_C(p)$, where p is the partial O_2 pressure, C is the relative spectral contribution of molecule C to the total absorption, $Y_{AB}(p)$ is the fractional saturation of the sum of molecule A and B, and $Y_C(p)$ is the fractional saturation of molecule C. The model assumes that molecules A and B show a similar high O_2 affinity without cooperativity, and thus $Y_{AB}(p)$ is defined as

$$Y_{AB}(p) = \frac{K_{AB}p}{1 + K_{AB}p} \quad (1)$$

where K_{AB} is the O_2 association equilibrium constant for molecules A and B. The model also assumes that molecule C shows a sample-

dx.doi.org/10.1021/ja500380e | J. Am. Chem. Soc. 2014, 136, 5097−5105

dependent affinity and cooperativity, and thus $Y_C(p)$ for HL− and HL+ is defined as

$$Y_C(p) = \frac{K_1 p + K_1 K_2 p^2}{1 + 2K_1 p + K_1 K_2 p^2} \quad (2)$$

where K_1 and K_2 are the first and second O_2 association equilibrium constants, respectively (HL− and HL+ contain two Fe(II)-hemes per tetramer). On the other hand, for FL+, a complete description requires a four-step Adair reaction scheme, and thus $Y_C(p)$ for FL+ is defined as

$$Y_C(p) = \frac{K_1 p + 3K_1 K_2 p^2 + 3K_1 K_2 K_3 p^3 + K_1 K_2 K_3 K_4 p^4}{1 + 4K_1 p + 6K_1 K_2 p^2 + 4K_1 K_2 K_3 p^3 + K_1 K_2 K_3 K_4 p^4} \quad (3)$$

where K_i is the i-th O_2 association equilibrium constant (i = 1−4). The determined O_2 affinities for the nine structures, namely, K_{AB} and K_2 (for molecule C of HL+ and HL−) or K_4 (for molecule C of FL+), are listed in Table 2. Note that the affinity of molecule C in FL+ cannot be determined accurately because of the number of parameters.

RESULTS AND DISCUSSION

In order to characterize crystallographically the entire allosteric pathway, we employed a novel crystal form capable of capturing multiple equilibrium conformers. This crystal form was identified in the course of our crystallization trials of various ligation states of human hemoglobin with and without anions using polyethylene glycol (PEG) as precipitant. We used β−β cross-linked Fe(II)−Ni(II) hybrids as models for partially liganded hemoglobins, based on previous findings that Ni(II)-heme is an excellent surrogate for deoxy Fe(II)-heme[30,31] and that fumaryl cross-linking between the two Lys82β residues (to prevent dimerization) does not affect the structure and function of human hemoglobin.[20,21,32] We found that three hemoglobin samples (see Figure 2), namely, XL[α(Fe-CO)β(Ni)][α(Ni)β-(Fe-CO)] with and without phosphate (referred to as HL+ and HL−, respectively) and fully water-liganded met-hemoglobin with phosphate (referred to as FL+), crystallize in the same $C2$ space group with comparable cell parameters (Table 1). Although the crystal structure of FL+ was previously solved by another group at 3.2 Å resolution,[24] the 2.75 Å-resolution structure presented here is more appropriate for comparison with the structures of HL+ and HL− determined at comparable (2.5−2.8 Å) resolutions. The crystallographic parameters are summarized in Table 1.

Two significant findings emerged. First, we found that each crystal structure captured the hemoglobin molecule in three different quaternary conformations in the asymmetric unit (Figure 2). The assignments of quaternary states are based on difference distance matrices of the $\alpha 1\beta 2$ subunits using R as a reference (Figure 3a and Table 2). Also, a quaternary deviation from R can be measured by superimposing the Cα atoms of the $\alpha 1\beta 1$ dimer of each structure on those of R, and calculating the root-mean-square deviation (RMSD) in the Cα atoms for the nonsuperimposed $\alpha 2\beta 2$ dimers (Figure 3b). In addition, the quaternary motion can be quantified as dimer−dimer rotation (Figure 1a), which is defined in terms of dimer−dimer rotation angle, rotation translation, and the direction of the rotation axis. These structural parameters support our assignments of quaternary states (Table 2). For example, in the HL+ crystal the three independent tetramers, termed molecules A, B, and C (Figure 2), assume R2, R, and T states, respectively, indicating that HL+ exists as an ensemble of very different quaternary conformations (Figure 3a,b and Table 2).

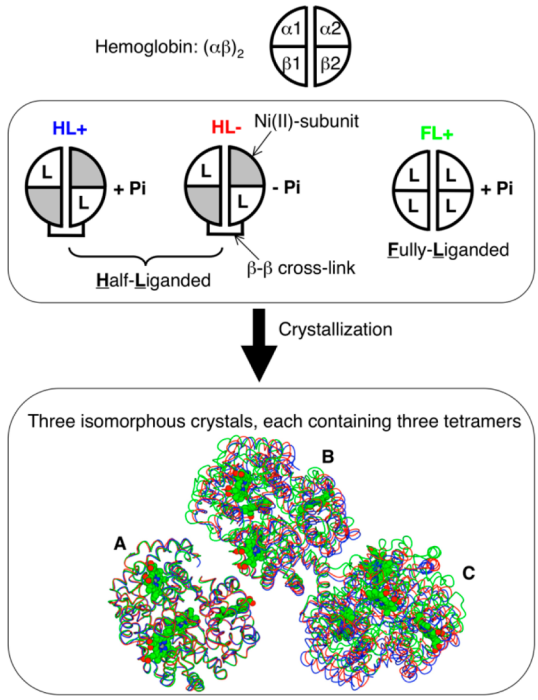

Figure 2. Three hemoglobin samples that crystallize in the same crystal form. The three hemoglobin samples are identified by color: blue (HL+), red (HL−), and green (FL+). L is ligand and Pi is phosphate. For HL+ and HL−, the β−β cross-link prevents dimerization, through which the original asymmetric tetramer is converted to two symmetric molecules. The three crystallographically independent molecules are termed A, B, and C. The captured nine structures are shown as a wire diagram by superimposing the Cα atoms of molecules A.

Another significant finding was that the conformations of molecules A, B, and C varied by hemoglobin ligation state and the presence or absence of phosphate, thereby leading to the nine conformers in the three isomorphous crystals to be structurally different from one another (Figures 3a,b and 4). These unprecedented features of this crystal form allow it to capture the ensemble of structures spanning the full range of ligation as snapshots of different conformers at equilibrium. As shown in Figure 3a, the gradual color progression from T-pattern to R-pattern (without color) to R2-pattern demonstrates the existence of a nearly continuous distribution of quaternary structures spanning from T to R to R2 (see also Figure 4). Among them, we identified a previously unidentified intermediate between T and R (called TR) found for molecule C in HL− (exhibiting a weak T-pattern in Figure 3a, and shown in Figure 5), as well as a series of relaxed intermediates between R and R2 (Figure 3a). This demonstration of multiple snapshot structures using a single crystal form is much more convincing evidence of coexisting forms than previous analyses comparing different crystal forms grown under different conditions.

Our structural results are consistent with recent global analyses of hundreds of known crystal structures of human hemoglobin in Protein Data Bank (PDB),[33,34] showing that these structures can be arranged orderly along a major pathway from T to R to R2, with a few exceptions such as R3 (that may be off this pathway),[8] although a wide gap appears between T and R (as no structure is available between T and R). Our discovery of TR may fill this gap, providing further support of the major allosteric pathway from T to R to R2.

dx.doi.org/10.1021/ja500380e | J. Am. Chem. Soc. 2014, 136, 5097−5105

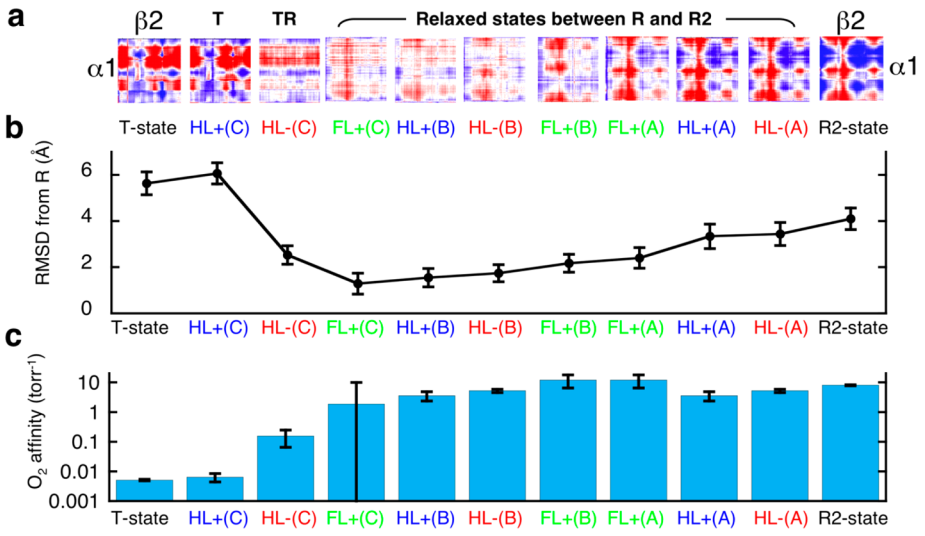

Figure 3. Nine distinct conformations of human hemoglobin in a single crystal form. For comparison, R2-state CO-bound hemoglobin (rightmost; PDB ID 1BBB) and T-state deoxyhemoglobin (leftmost; PDB ID 2DN2) are also shown. (a) Difference distance matrices of the $\alpha 1\beta 2$ subunits using R-state CO-bound hemoglobin (PDB ID 2DN3) as a reference. Red regions represent residues that move closer in the target structure relative to R, whereas the opposite happens in the blue regions. (b) RMSD in the Cα atoms of the $\alpha 2\beta 2$ dimers after superimposing the Cα atoms of the $\alpha 1\beta 1$ dimer of each structure on those of R-state CO-bound hemoglobin. Each bar indicates RMSD in the Cα atoms of the superimposed $\alpha 1\beta 1$ dimers. (c) O_2 affinities in crystallo of the nine conformations (derived from Figure 7a).

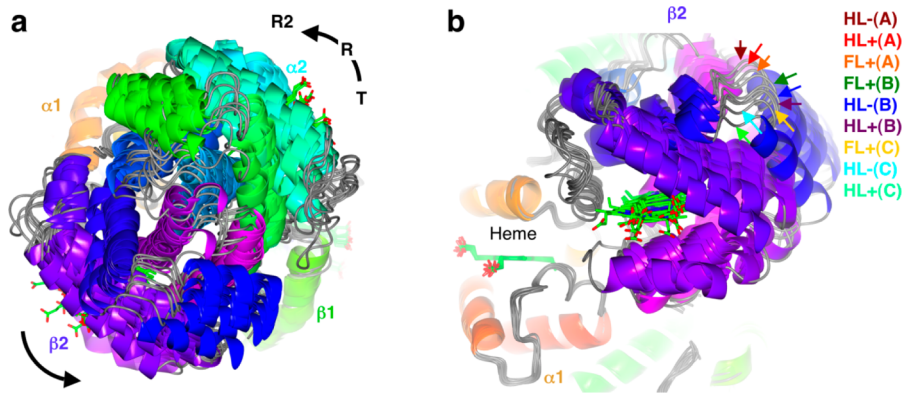

Figure 4. Comparison of the nine quaternary structures. (a) Ribbon diagram showing the orientation of the $\alpha 2\beta 2$ dimers relative to the $\alpha 1\beta 1$ dimers in the nine conformations. The Cα atoms of the $\alpha 1\beta 1$ dimers in all the structures are superimposed. (b) Close-up view of the $\beta 2$ subunits in the same nine structures as (a), but from a different viewing angle.

We next used microspectrophotometry to determine the O_2 affinity in crystallo of each of the nine tetramer structures. After the crystals were converted to the oxy form, they were equilibrated with controlled O_2 pressures and absorption spectra were measured with light incident on the (010) crystal face. The fractional saturation with O_2 was calculated by a least-squares fit of the observed absorption spectra to a linear combination of the reference spectra of the oxy-, deoxy-, and met-forms of the same crystal (Figure 6). Figure 7a shows the Hill plots of O_2 dissociation curves for the HL+, HL−, and FL+ crystals. Reversibility was confirmed by agreement between the O_2 dissociation data and the corresponding association data (Figure 7b). Interestingly, all the crystals show a biphasic equilibrium curve with two components of comparable amplitude: one shows a very high O_2 affinity with little or no cooperativity (the left half of the Hill plot), and the other shows a sample-dependent affinity and cooperativity (the right half of the Hill plot). We interpret this observation to mean that the noncooperative high-affinity component arises from molecules A and B, while the other from molecule C (as indicated in Figure 7b) for the following reasons: (i) As shown in Figure 3a, the conformations of A and B vary only within the range of relaxed states (from R to R2), whereas the conformation of C varies from T (HL+) to R (FL+) through TR (HL−), suggesting a sample-dependent O_2 affinity and possible cooperativity. (ii) No significant change in O_2 affinity during the R → R2 transition has been supported by the recent finding[15] that both of the R and R2 crystals show a similar very high O_2 affinity (see Figure 1b). (iii) In our crystals, molecules A, B, and C make different contributions to light absorption in an approximate ratio of 2:3:4 in amplitude (Table 2), in agreement with the amplitudes of our assigned two components (A + B and C). According to this biphasic model, all the O_2 dissociation curves were indeed well fitted (Figure 7a,b). Note that since it has been shown that the α and β subunits have nearly equal O_2 affinities regardless of the quaternary states,[11,13,15,16,36,37] our analyses assume no differences in the O_2 affinities of both subunits in all the tetramers. The determined O_2 affinities of the nine conformations are shown in Figure 3c and listed in Table 2.

Our results show that all the relaxed states, from classical R to R2, have the same high O_2 affinity and that the reduction in O_2

dx.doi.org/10.1021/ja500380e | J. Am. Chem. Soc. 2014, 136, 5097−5105

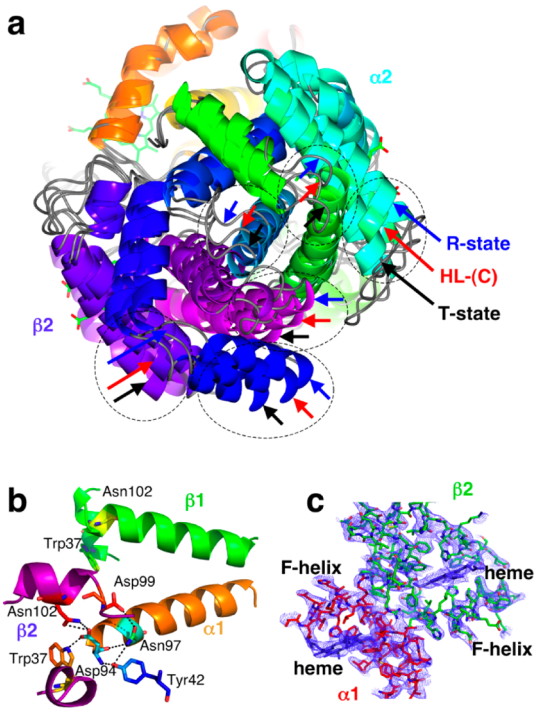

Figure 5. Structure of a new intermediate TR that lies between T and R. (a) Molecule C in HL− assumes TR. The $\alpha 2\beta 2$ dimers of T, TR, and R are indicated by black, red, and blue arrows, respectively. The Cα atoms of the $\alpha 1\beta 1$ dimers are superimposed. (b) Structure around the $\alpha 1\beta 2$ interface of TR. The residues involved in hydrogen bonds (dashed lines) are shown as a stick model. (c) Electron density map for the $\alpha 1\beta 2$ interface of TR. The $2F_o-F_c$ electron density map contoured at 1.0σ is shown as a blue mesh. The residues in the $\alpha 1$ and $\beta 2$ subunits are shown as red and green sticks, respectively, with the heme groups shown as blue sticks.

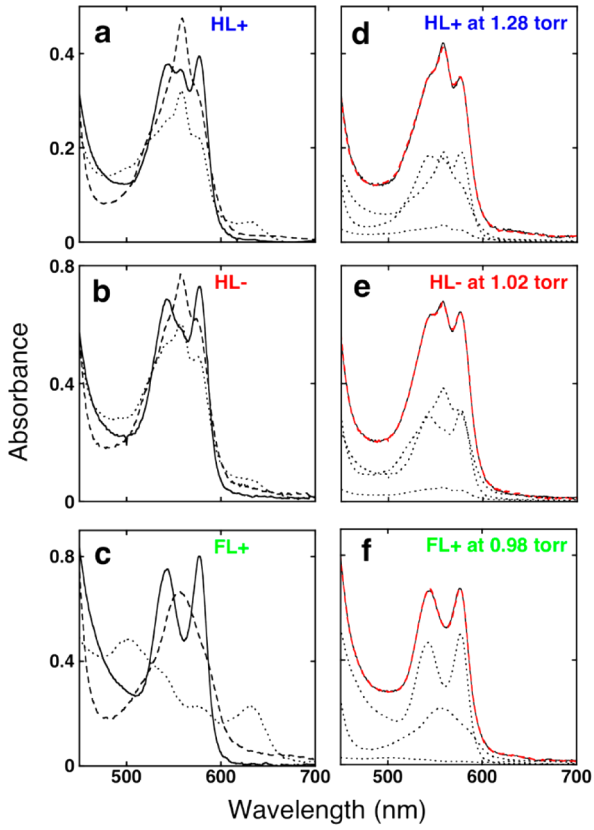

Figure 6. Determination of the fractional saturation with O_2 of the ferrous hemes (Y) in the HL+, HL−, and FL+ crystals. (a−c) Reference absorption spectra of the HL+, HL−, and FL+ crystals, measured with light incident on the (010) crystal face. In each panel, the spectra of the oxy-, deoxy-, and met-forms are shown as solid, dashed, and dotted curve, respectively. (d−f) Examples of the fitting. The fractional saturation of the ferrous hemes with O_2 (Y) was calculated by a least-squares fit of the observed absorption spectrum to a linear combination of three reference spectra (a−c) and a baseline offset. The solid black curves are the observed spectra, the dashed red curves are the sums of the component reference spectra, and the dotted black curves are the component reference spectra. The fractional amounts of oxy-, deoxy-, and met-forms are calculated to be 48.6, 40.3, and 11.1%, respectively, for the HL+ crystal equilibrated with O_2 at a pressure of 1.28 Torr (shown in d), 42.1, 50.0, and 7.9%, respectively, for the HL− crystal at 1.02 Torr (shown in e), and 62.1, 32.4, and 5.5%, respectively, for the FL + crystal at 0.98 Torr (shown in f).

affinity could occur only in the transition pathway from R to T (Figure 3 and Table 2). This implies that relaxed-state tetramers with a loosely packed dimer−dimer interface bind O_2 with nearly the same high affinity as the $\alpha 1\beta 1$ dimer,[38] as well as the isolated α and β subunits,[39] confirming the central importance of quaternary constraints in tetrameric hemoglobin to its cooperativity. It is also confirmed that the $\alpha 1\beta 1$ dimer interface is almost unchanged regardless of quaternary states, as judged by the small RMSD in the Cα atoms of the $\alpha 1\beta 1$ dimer (bars in Figure 3b), and the difference distance matrices of the $(\alpha 1\beta 1)(\alpha 2\beta 2)$ subunits (Figure 8).

Although the $\alpha 1\beta 1$ and $\alpha 2\beta 2$ dimers in asymmetric XL[α(Fe-CO)β(Ni)][α(Ni)β(Fe-CO)] (HL+ or HL−) are not equivalent in terms of ligation state, crystal lattices appear not to discriminate between them because the relative spectral contributions of molecule C are close to the values expected from randomly placed dimers (Table 2). This is consistent with a recent study showing that both the asymmetrically half-liganded tetramers, XL[α(Fe-CO)β(Ni)][α(Ni)β(Fe-CO)] and XL[α-(Fe-CO)β(Fe-CO)][α(Ni)β(Ni)], are only slightly distorted from the perfect 2-fold symmetry by asymmetric ($\alpha 1\beta 2$ or $\alpha 1\beta 1$) ligation,[40] supporting a key assumption of the MWC model.[3] Thus, in this study, we only focus on the quaternary structures of the observed conformers rather than the details of tertiary structural differences among them.

The structure and function of the new intermediate TR reveal features that could explain a long-standing question regarding the functional plasticity of the T-state (Figure 1b). It has long been recognized that K_T varies widely with solution conditions,[16−19,41,42] from a low of 0.0057 Torr^{-1} to a high of 0.24 Torr^{-1} at 20 °C.[33] This affinity variation is physiologically important because it accounts for a significant part of the alkaline Bohr effect of human hemoglobin (Figure 1b). However, so far all known quaternary structures of crystalline T-state are essentially the same and retain intact Bohr group salt-bridges, even though a wide range of crystallization conditions have been identified.[33,34] Also, the O_2 affinity of the crystalline T-state is independent of solvent conditions and identical to the lowest K_T value in solution (Figure 1b), implying that the canonical T-state represents the lowest affinity state in solution.[16] Thus, the important missing link is an as yet unidentified allosteric state with intermediate O_2 affinity (corresponding to the highest K_T value),[16−19] broken Bohr group salt-bridges,[16,17] and free of bound anions.[18] We now identify TR as such a candidate. In fact, TR is crystallized without anions and exhibits an intermediate O_2 affinity (0.16 ± 0.09 Torr^{-1}) compatible with the highest K_T

dx.doi.org/10.1021/ja500380e | J. Am. Chem. Soc. 2014, 136, 5097−5105

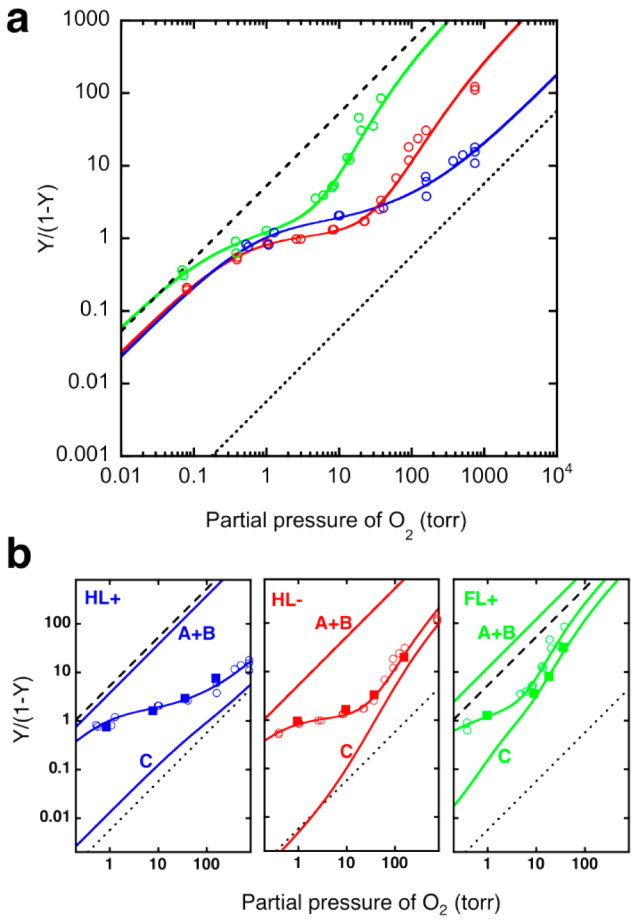

Figure 7. O_2 equilibrium data for the HL+, HL−, and FL+ crystals. (a) Hill plots of O_2 dissociation curves for the crystals of HL+ (blue), HL− (red), and FL+ (green). The solid curves through data points represent the least-squares fits with the biphasic model. The dashed and dotted lines represent the highest and lowest O_2 affinities of solution hemoglobin, respectively, at 20 °C.[35] (b) Hill plots showing reversibility and two functional components in each crystal. O_2 dissociation data (open circles) and the corresponding association data (filled squares) are compared. The colored lines labeled as "A + B" and "C" represent the simulated O_2 equilibrium curves for the sum of molecules A and B, and those for molecule C, respectively.

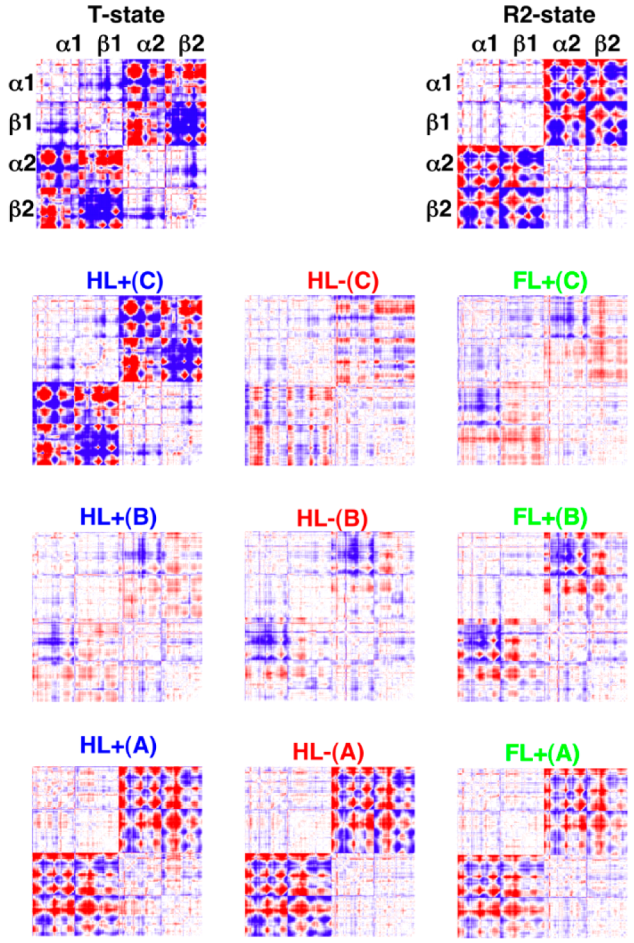

Figure 8. Difference distance matrices of the $(\alpha1\beta1)(\alpha2\beta2)$ subunits. Reference structure and the definitions of colors are same as in Figure 3a.

Table 3. Distances between the Residues Involved in Salt Bridges and Hydrogen Bonds in TR, T, and R[a]

residues	TR	T	R
salt bridges			
Arg141α1-Asp126α2	–	2.78 (2.66)	–
Lys40α1-His146β2	–	2.83 (2.59)	–
Asp94β1-His146β1	–	2.60 (2.84)	–
hydrogen bonds			
switch region			
Tyr42α1-Asp99β2	–	2.51 (2.52)	–
Asn97α1-Asp99β2	3.63 (3.22)	2.85 (2.82)	4.46
Asp94α1-Asn102β2	3.17 (3.38)	–	2.74
hinge region			
Asp94α1-Trp37β2	2.70 (3.29)	2.85 (2.84)	3.67
Trp37β1-Asn102β1	3.78 (3.39)	–	2.95
intra-α-subunit			
Asn97α1-Asp94α1 (CO)	3.55 (3.39)	3.04 (3.03)	3.61
Tyr42α1-Asp94α1 (NH)	2.40 (3.20)	2.99 (3.01)	3.02
Tyr42α1-Asn97α1	3.54 (3.61)	3.45 (3.41)	3.25

[a]All distances are shown in Angstrom units. Values in parentheses are distances for noncrystallographic symmetry equivalent bonds. A dash indicates a distance longer than 5 Å.

value (0.24 $Torr^{-1}$). The Bohr group salt-bridges are broken as in the R state, but a characteristic hydrogen bond of the T-state between Asp94α1 and Trp37β2 is retained (Figure 5b and Table 3). This bond, at the hinge region of the $\alpha1\beta2$ interface, is a key constraint on the T-state.[43] We should note here that despite its importance, the stereochemistry around the heme groups in TR is difficult to evaluate, because of low resolution, and also because crystal lattices do not discriminate between the two inequivalent dimers of asymmetric XL[α(Fe-CO)β(Ni)][α(Ni)β(Fe-CO)] (as described above).

Previous O_2 equilibrium studies on T-state crystals of des-Arg141α hemoglobin (hemoglobin modified by removal of the α chain C-terminal residue, Arg141α) and des-His146β hemoglobin (hemoglobin modified by removal of the β chain C-terminal residue, His146β) provide strong evidence that the salt-bridges associated with the C-terminal Arg141α and His146β are a key determinant of the low affinity of crystalline T-state.[44,45] These studies show that in the T structure the removal of Arg141α (eliminating the α salt-bridges) is associated with a 15-fold increase in the O_2 affinity,[44] whereas the removal of His146β (eliminating the β salt-bridges) results in a 1.7-fold increase in the O_2 affinity.[45] It is interesting to note that the O_2 affinity of TR is 28-fold higher than that of the crystalline T-state, which is

dx.doi.org/10.1021/ja500380e | J. Am. Chem. Soc. 2014, 136, 5097−5105

comparable to the affinity change associated with the removal of both α and β salt-bridges.

The achievement of capturing TR is not a consequence of cross-linking. In fact, molecule C in the HL+ crystal assumes a typical T conformation while carrying the $\beta-\beta$ cross-link (Figures 3a and 8; Table 2). Furthermore, the O_2 equilibrium properties of $\beta-\beta$ cross-linked hemoglobin are very similar to those of unmodified hemoglobin with respect to O_2 affinity, cooperativity, and the alkaline Bohr effect.[20] This is in marked contrast to the previous X-ray study of Schumacher et al.,[46] where different types of cross-linked hemoglobins with low O_2 affinity were used to capture transient intermediates by preventing complete allosteric transition into the R state. Overall, our results indicate that TR is a fundamental part of the allosteric regulation mechanism of human hemoglobin.

Finally, this study presents an important example of human hemoglobin crystals that allow reversible structural changes of the protein, as evidenced by the reversible and cooperative O_2 dissociation curves (Figure 7a,b). Specifically, molecules C in HL− and FL+ bind O_2 cooperatively with a Hill coefficient of 1.7, while that in HL+ binds O_2 in a noncooperative fashion (Figure 7b). Thus, the use of the HL− or FL+ crystals would make it possible to perform a dynamic X-ray analysis of the hemoglobin allosteric transition by changing the O_2 saturation.

CONCLUSION

The combined usage of metal-substitution and interdimer chemical cross-linking allows us to investigate various ligation states of human hemoglobin in pure forms. We show that XL[α(Fe-CO)β(Ni)][α(Ni)β(Fe-CO)] with and without phosphate (HL+ and HL−) and fully water-liganded met-hemoglobin with phosphate (FL+) crystallize in the same crystal form, in which hemoglobin is free to adopt any allosteric structure, depending on the conditions, and at the same time allows O_2 binding to be monitored directly in the crystal. We identify nine different equilibrium conformers that cover the complete conformational space of hemoglobin, providing clear and convincing evidence of coexisting states.

Our results strongly suggest that concerted transitions do occur in hemoglobin, and thus favor the MWC-like pre-existing equilibrium models over the sequential induced-fit models proposed by Pauling[47] and Koshland−Nemethy−Filmer (KNF).[48] Various extension of the simple two-state MWC model have been proposed to include the solution-dependent O_2 affinity of the hemoglobin quaternary state(s).[17,49−51] In general, there are two ways to incorporate the functional plasticity of the T-state in the model, either by allowing the tertiary structural changes within the quaternary T state (modified two-state model),[49−51] or by introducing a third allosteric state with an intermediate O_2 affinity (three-state model).[16−19] Clearly, our discovery of TR is better accounted for by the three-state model rather than by the modified two-state model, although the debate still continues.

The observation that hemoglobin exists in equilibrium between multiple, not only two, conformations is not inconsistent with the original MWC model[3] that assumes two (at least two) states reversibly accessible to allosteric oligomers. Although the number of allosteric states was not restricted by the original model, its simplest version with only two-states has so far been taken up with enthusiasm by many researchers. Thus, the discovery of a new allosteric state (TR) of human hemoglobin is an important reminder that allosteric proteins may have multiple quaternary structures that are functionally different.

AUTHOR INFORMATION

Corresponding Author

shibayam@jichi.ac.jp

Notes

The authors declare no competing financial interest.

ACKNOWLEDGMENTS

We thank the staff at the beam-line BL17A of the Photon Factory for assistance with data collection. This work was supported by JSPS KAKENHI Grant Number 23570197 to N.S.

REFERENCES

(1) Baldwin, J.; Chothia, C. *J. Mol. Biol.* **1979**, *129*, 175−220.
(2) Perutz, M. F. *Q. Rev. Biophys.* **1989**, *22*, 139−237.
(3) Monod, J.; Wyman, J.; Changeux, J. P. *J. Mol. Biol.* **1965**, *12*, 88−118.
(4) Silva, M. M.; Rogers, P. H.; Arnone, A. *J. Biol. Chem.* **1992**, *267*, 17248−17256.
(5) Janin, J.; Wodak, S. J. *Proteins* **1993**, *15*, 1−4.
(6) Srinivasan, R.; Rose, G. D. *Proc. Natl. Acad. Sci. U. S. A.* **1994**, *91*, 11113−11117.
(7) Tame, J. R. H. *Trends Biochem. Sci.* **1999**, *24*, 372−377.
(8) Safo, M. K.; Abraham, D. J. *Biochemistry* **2005**, *44*, 8347−8359.
(9) Lukin, J. A.; Kontaxis, G.; Simplaceanu, V.; Yuan, Y.; Bax, A.; Ho, C. *Proc. Natl. Acad. Sci. U. S. A.* **2003**, *100*, 517−520.
(10) Makowski, L.; Bardhan, J.; Gore, D.; Lal, J.; Mandava, S.; Park, S.; Rodi, D. J.; Ho, N. T.; Ho, C.; Fischetti, R. F. *J. Mol. Biol.* **2011**, *408*, 909−921.
(11) Mozzarelli, A.; Rivetti, C.; Rossi, G. L.; Henry, E. R.; Eaton, W. A. *Nature* **1991**, *351*, 416−419.
(12) Imai, K. *J. Mol. Biol.* **1979**, *133*, 233−247.
(13) Rivetti, C.; Mozzarelli, A.; Rossi, G. L.; Henry, E. R.; Eaton, W. A. *Biochemistry* **1993**, *32*, 2888−2906.
(14) Mozzarelli, A.; Rivetti, C.; Rossi, G. L.; Eaton, W. A.; Henry, E. R. *Protein Sci.* **1997**, *6*, 484−489.
(15) Shibayama, N.; Sugiyama, K.; Park, S. Y. *J. Biol. Chem.* **2011**, *286*, 33661−33668.
(16) Miyazaki, G.; Morimoto, H.; Yun, K. M.; Park, S. Y.; Nakagawa, A.; Minagawa, H.; Shibayama, N. *J. Mol. Biol.* **1999**, *292*, 1121−1136.
(17) Minton, A. P.; Imai, K. *Proc. Natl. Acad. Sci. U. S. A.* **1974**, *71*, 1418−1421.
(18) Colombo, M. F.; Seixas, F. A. V. *Biochemistry* **1999**, *38*, 11741−11748.
(19) Shibayama, N.; Saigo, S. *FEBS Lett.* **2001**, *492*, 50−53.
(20) Shibayama, N.; Imai, K.; Hirata, H.; Hiraiwa, H.; Morimoto, H.; Saigo, S. *Biochemistry* **1991**, *30*, 8158−8165.
(21) Shibayama, N.; Imai, K.; Morimoto, H.; Saigo, S. *Biochemistry* **1995**, *34*, 4773−4780.
(22) Benesch, R.; Benesch, R. E.; Macduff, G. *Science* **1964**, *144*, 68−69.
(23) Otwinowski, Z.; Minor, W. *Methods Enzymol.* **1997**, *276*, 307−326.
(24) Biswal, B. K.; Vijayan, M. *Curr. Sci.* **2001**, *81*, 1100−1105.
(25) Collaborative Computational Project, Number 4. *Acta Crystallogr., Sect. D: Biol. Crystallogr.* **1994**, *50*, 760−763.
(26) Park, S. Y.; Yokoyama, T.; Shibayama, N.; Shiro, Y.; Tame, J. R. H. *J. Mol. Biol.* **2006**, *360*, 690−701.
(27) Emsley, P.; Cowtan, K. *Acta Crystallogr., Sect. D: Biol. Crystallogr.* **2004**, *60*, 2126−2132.
(28) Brünger, A. T.; Adams, P. D.; Clore, G. M.; DeLano, W. L.; Gros, P.; Grosse-Kunstleve, R. W.; Jiang, J. S.; Kuszewski, J.; Nilges, M.; Pannu, N. S.; Read, R. J.; Rice, L. M.; Simonson, T.; Warren, G. L. *Acta Crystallogr., Sect. D: Biol. Crystallogr.* **1998**, *54*, 905−921.
(29) Laskowski, R. A.; Moss, D. S.; Thornton, J. M. *J. Mol. Biol.* **1993**, *231*, 1049−1067.
(30) Shibayama, N.; Morimoto, H.; Miyazaki, G. *J. Mol. Biol.* **1986**, *192*, 323−329.

(31) Shibayama, N.; Morimoto, H.; Kitagawa, T. *J. Mol. Biol.* **1986**, *192*, 331−336.
(32) Park, S. Y.; Shibayama, N.; Hiraki, T.; Tame, J. R. H. *Biochemistry* **2004**, *43*, 8711−8717.
(33) Dey, S.; Chakrabarti, P.; Janin, J. *Proteins* **2011**, *79*, 2861−2870.
(34) Ren, Z. *PLoS One* **2013**, *8*, e77141.
(35) Shibayama, N. In *Hemoglobin: Recent Developments and Topics*; Nagai, M., Ed.; Research Signpost: Trivandrum, India, 2011; pp 123−142.
(36) Sawicki, C. A.; Gibson, Q. H. *J. Biol. Chem.* **1977**, *252*, 7538−7547.
(37) Philo, J. S.; Lary, J. W. *J. Biol. Chem.* **1990**, *265*, 139−143.
(38) Hewitt, J. A.; Kilmartin, J. V.; Eyck, L. F. T.; Perutz, M. F. *Proc. Natl. Acad. Sci. U. S. A.* **1972**, *69*, 203−207.
(39) Tyuma, I.; Shimizu, K.; Imai, K. *Biochem. Biophys. Res. Commun.* **1971**, *43*, 423−428.
(40) Shibayama, N. *FEBS Lett.* **2012**, *586*, 74−78.
(41) Poyart, C. F.; Bursaux, E.; Bohn, B. *Eur. J. Biochem.* **1978**, *87*, 75−83.
(42) Kilmartin, J. V.; Imai, K.; Jones, R. T.; Faruqui, A. R.; Fogg, J.; Baldwin, J. M. *Biochim. Biophys. Acta* **1978**, *534*, 15−25.
(43) Mihailescu, M. R.; Fronticelli, C.; Russu, I. M. *Proteins* **2001**, *44*, 73−78.
(44) Kavanaugh, J. S.; Chafin, D. R.; Arnone, A.; Mozzarelli, A.; Rivetti, C.; Rossi, G. L.; Kwiatkowski, L. D.; Noble, R. W. *J. Mol. Biol.* **1995**, *248*, 136−150.
(45) Bettati, S.; Kwiatkowski, L. D.; Kavanaugh, J. S.; Mozzarelli, A.; Arnone, A.; Rossi, G. L.; Noble, R. W. *J. Biol. Chem.* **1997**, *272*, 33077−33084.
(46) Schumacher, M. A.; Dixon, M. M.; Kluger, R.; Jones, R. T.; Brennan, R. G. *Nature* **1995**, *375*, 84−87.
(47) Pauling, L. *Proc. Natl. Acad. Sci. U. S. A.* **1935**, *21*, 186−191.
(48) Koshland, D. E.; Nemethy, G.; Filmer, D. *Biochemistry* **1966**, *5*, 365−385.
(49) Szabo, A.; Karplus, M. *J. Mol. Biol.* **1972**, *72*, 163−197.
(50) Henry, E. R.; Bettati, S.; Hofrichter, J.; Eaton, W. A. *Biophys. Chem.* **2002**, *98*, 149−164.
(51) Yonetani, T.; Park, S.; Tsuneshige, A.; Imai, K.; Kanaori, K. *J. Biol. Chem.* **2002**, *277*, 34508−34520.